Investigating The Fatigue Behaviour of High-Temperature Annealed LPBF Ti6Al4V(ELI) Tested At Elevated Temperatures

Tumelo Moloi [1,*] and Thywill Cephas Dzogbewu [1]

[1]Department of Mechanical and Mechatronics Engineering, Central University of Technology, Free State, Private Bag X20539, Bloemfontein 9300, South Africa
Maina Maringa [2] and Amos Muiruri [2]
[1]Department of Mechanical Engineering, Murang'a University of Technology, P.O. Box 75-10200, Murang'a, Kenya
*Corresponding author.
Email address: moloitd7@gmail.com

Abstract: Though failure of engineering materials has been studied extensively, the prevention of failure is never guaranteed. In many high-temperature industries, engineering structures often experience fatigue failure due to temperature fluctuations. The present study aims to investigate the effect of elevated temperatures on the fatigue life of Ti6Al4V(ELI). In this study, an LPBF EOSINT M290 machine was used to manufacture test specimens. The results obtained showed that elevated temperatures above room temperature, till 325 °C, have an insignificant effect on the fatigue life of Ti6Al4V(ELI) specimens.

Keywords: Fatigue behaviour, Elevated temperatures, LPBF Ti6Al4V(ELI), Fracture surface, Porosity.

1. Introduction

Stability at high temperatures is necessary for a number of applications. For high-temperature applications, metals and metal alloys require a particular combination of mechanical strength, microstructure, and corrosion resistance [1]. An alloy is considered high temperature alloy if it remains functional at 500 °C and higher. Testing at high temperatures may affect the material's fatigue properties. Metals and their alloys undergo a decrease in fatigue strength when their operating temperature is raised [2]. Tokaji [3], studied the effect of elevated temperature on the fatigue life of Ti6Al4V alloy, at room temperature and at 623 K and 723 K, and reported that fatigue strength decreases with increasing temperature [3]. Arakere et al. [4], studied the behaviour of Ti6Al4V at room temperature, 175, 230, 290, and 345 °C. They observed no significant change in the rates of crack growth due to these varying temperatures [4]. Jiao et al. [5], compared the fatigue crack resistance of SLM Ti6Al4V tested at room temperature and at 400 °C, and found that the fatigue crack growth rate was higher at the latter than at the former test temperatures [5].

An additive manufacturing technique called laser powder bed fusion selectively melts powder to produce parts by using a laser as an energy source. This technology is among the most adaptable and promising methods for manufacturing metal [6]. The technique uses a high-energy laser beam to create parts from 3D model data. This technology has the ability to fabricate complicated structures consisting of interconnected parts with little wastage of material [7]. Additionally, this technique can accurately create thin walls and fine features [8]. Laser powder bed fusion has been used widely to produce Ti6Al4V(ELI) parts [9]. The Ti6Al4V alloy is a dual-phase (α+β) alloy of titanium that possesses high specific strength, low density, high fracture toughness, good corrosion resistance, and biocompatibility [10]. The alloy is used for numerous applications in a variety of sectors, including the aerospace, biomedical, and automobile [11]. The Ti6Al4V alloy is commonly used at normal room temperature and up to temperatures of 250-400 °C [12]. In the high-cycle fatigue regime, the porosity of parts manufactured through laser powder bed fusion that results from un-melted or semi-melted powder, as well as surface roughness, influences the fatigue behaviour of the parts, thus reducing their fatigue life [7]. Extensive research has been conducted on the fatigue life of metals and the factors impacting it. However, there has been limited investigation into how elevated temperatures affect their fatigue life.

This study aims to examine the influence of high temperatures on the fatigue life of high-temperature annealed Ti6Al4V(ELI). To improve the accuracy of fatigue life prediction for additively manufactured parts, determine the fatigue fracture behaviour, determine the significance of the post-heat treatment process suited to resist fatigue at elevated temperature, and contribute to the empirical data to support the certification of LPBF Ti6Al4V parts for elevated temperature application.

2. Methodology

2.1. Preparation of samples

All of the fatigue Ti6Al4V (ELI) test specimens were manufactured using the LPBF EOSINT M290 machine. The specimens were manufactured as rods with a diameter of 12 mm and a length of 81 mm. The machine was set up to create Ti6Al4V (ELI) parts according to the manufacturer's recommended process parameters, as indicated in Table 1, and the specimens used in this work were built vertically. The samples were produced at the Central University of Technology Free State's Center for Rapid Prototyping (CRPM).

Table 1: Process parameters for Ti6Al4V(ELI) manufactured by LPBF EOSINT M290

Parameters	Laser power (W)	Hatch spacing (μm)	Layer thickness (μm)	Scanning speed (mm/s)	Laser diameter (μm)
Ti6Al4V(ELI)	280	120	40	1300	80-100

2.2. Post-Heat Treatment Processes

Following additive manufacturing, specimens were subjected to high-temperature annealing and stress-relieving heat treatments. While the specimens were still affixed to the building substrate, stress relief and high-temperature annealing were carried out. The specimens were heated to 600 °C at a rate of 0.08 °C/s for three hours in order to relieve stress. After that, they were cooled in a furnace to room temperature. Thereafter, the specimens were exposed to high-temperature annealing. In this process, the specimens were heated to 990 °C at a rate of 0.13 °C/s and maintained there for an hour. After that, they were cooled in a furnace to 705 °C for two hours before being cooled in the furnace back to room temperature. The temperature of 980 °C was chosen to guarantee the transformation of the microstructure to α- and β-grains, and the soaking process was carried out at this temperature to guarantee that the final microstructure was homogenized. To guarantee the conversion of β-grains to α-grains and their enlargement to improve the alloy's ductility, furnace cooling at 705 °C was used. These post-heat treatment processes were conducted at the Center for Rapid Prototyping (CRPM), Central University of Technology Free State, Bloemfontein.

2.3. Machining of specimens

For fatigue testing, the specimens were machined in accordance with ASTM E466 standards. The specimen's dimensions are displayed in Figure 1. The specimens were machined at the Central University of Technology Free State's Product Development Technology Station (PDTS).

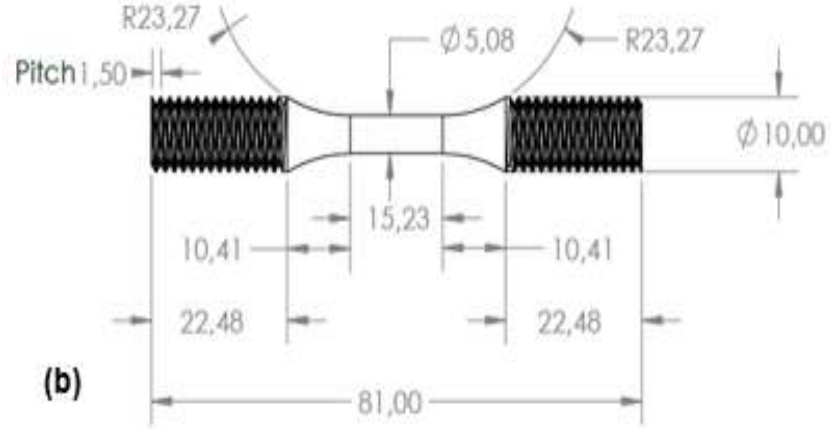


Figure 1: Test specimens for fatigue tension-tension

2.4. Fatigue testing

Fatigue tension-tension tests were conducted using an Instron 8801 servo-hydraulic testing frame. The equipment can be found at the University of South Africa in Johannesburg, South Africa's Roodepoort. Specimens were tested at three different temperatures: 20 °C, 175 °C, and 325 °C. At a test frequency of 25 Hz and a stress ratio, R, of 0.1, the cut-off maximum allowed number of test cycles was set at 5,000,000 cycles. One specimen is utilized for each of the maximum test stresses of 80, 70, 60, 50, 40, and 30% of the yield strength (tested in tension at various temperatures). Each specimen was placed on the testing equipment, heated to the desired test temperature, and then subjected to a tension-tension load until it failed or reached 5,000,000 cycles. One scaling factor that can be used to describe the stresses surrounding a crack is the stress intensity factor.

2.5. Fractography

A scanning electron microscope (SEM) was used to analyze the characteristics of failure on the fractured surfaces of the tested specimens to determine the cause and the characteristics of failure. The SEM analysis was carried out at the University of Free State, Bloemfontein, South Africa. A mount-plate was carefully used to carefully mount broken specimens simultaneously, leaving the fracture surface free for examination.

2.6. Micro-CT Scanning

The specimens that endured maximum stress till the attainment of 5,000,000 cycles without failure were taken for micro-CT scanning to examine the defects. A General Electric Phoenix VTomeX L240 X-ray CT system of Reconstruction - Phoenix Datos x Analysis - Volume Graphics VGSTUDIO MAX 2024 software was used. The Ti6AL4V(ELI) samples were scanned at a Voxel size of 10 µm, with a filter thickness of 0.3 mm Cu, a voltage of 110 kV, and a current of 90 µA. Micro-CT scanning was conducted at the University of Stellenbosch, Stellenbosch, South Africa. Consider a defect with a two-dimensional crack, length 2a in the x- and y-directions, under a uniaxial tensile stress σ_0. An infinite solid under uniform remote tensile stress, σ_0, in the z-direction is shown with an internal crack on the x-y plane [13]. For a singular stress distribution in the vicinity of the crack tip. The stress intensity, represented by the parameter K, is written as:

$$K = \sigma\sqrt{\pi a}$$

When the area of this defect is 'area', then the maximum value of the stress intensity factor, K_{Imax}, along the defect, is expressed as:

$$K = C\sigma\sqrt{\pi\sqrt{area}}$$

where the symbol C, is a dimensionless parameter taken as 0.5 for an internal defect and 0.65 for a defect on the surface, σ, is the maximum stress applied [41], [13]. The change in stress intensity factor is expressed:

$$\Delta K = C\Delta\sigma\sqrt{\pi\sqrt{area}}$$

2.7. Metallographic Examination

From the fractured fatigue specimen, an orthogonal piece was cut closer to the fracture surface, and another piece was cut far away from the fracture. The cut piece was mounted in Multifast resin inside a mounting cylinder using a Struers Mounting Press Citopress machine, freeing the orthogonal cut surfaces. These free surfaces were ground using a Struers tegramin machine with 320 grit silicon carbide (SiC) grinding paper and water for lubrication. Three stages of polishing were used to produce mirror-finish surfaces. A Struers tegramin machine was used to polish for five minutes using a Largo Diapro cloth and a 9 µm diamond suspension. After that, a Mol Diapro cloth was used for two minutes of polishing. Using an MD-Chem cloth with a 4 µm diamond suspension, the final polishing stage was finished in 110 seconds. Kroll's reagent (Water 92.82%, Nitric Acid 6.11%, and Hydrofluoric Acid 1.07%) was then used to etch the samples' polished surfaces. Etched surfaces that were still embedded in resin were then removed for metallographic analysis. The microstructures of the Ti6AL4V (ELI) samples were examined using an optical microscope. This was carried out at the Central University of Technology Free State, Bloemfontein, in the Material Laboratory located in the Yarona Building.

2.8. Vickers Microhardness

Vickers microhardness tests were performed using Future Tech FM 7E, FM7639 microhardness testing equipment. The selected polished and etched sample's surfaces were tested for microhardness at room

temperature. Ten indentations with a dwell duration of ten seconds and a test load of 2942 mN were carried out on each sample under the same conditions.

3. Results

3.1. Fatigue Properties

Table 2: Fatigue life of Ti6Al4V(ELI) specimens at different temperatures.

Specimen Number	Testing Temperature (°C)	Maximum Test Stress (MPa)	Area of a defect (mm^2)	Change in Stress Intensity Factor ($MPa.m^{0.5}$)	Number of Cycles to Failure or Runout
1	20	666.6	0.036	3.19	373,193
2	20	583.2	0.019	2.03	Runout
3	175	577.5	0.032	2.61	Runout
4	325	505.3	0.035	2.38	Runout

Table 2 shows that specimen 1, which was loaded to the highest maximum stress, endured 373,193 cycles before failure, whereas specimens 2-4 reached runout at 5,000,000 cycles. Similar to specimen 1, specimen 2 was tested at room temperature, though at lower test stresses, as expected, failure was anticipated at a much higher number of cycles than specimen 1. Reference [14], reported that the fatigue performance is reduced as the stress is increased. Surprisingly, only one specimen underwent fracture, and specimens 3 and 4 did not. The expectation was that specimens 3 and 4 tested at elevated temperatures would fail, as normally happens in fatigue testing conducted at elevated temperatures. This implies that the test temperatures were not high enough to cause failure. Zhao et al. [12], stated that Ti6Al4V is suited at temperatures below 400 °C, as temperatures above that would affect its microstructures and mechanical properties, which would ultimately lead to a reduction in its fatigue life. The results in Table 2 suggest an endurance limit of 583.2 MPa, as below this value, no failure was encountered. The endurance limit was found to be 483 MPa when Malefane et al. [15] tested the high-cycle fatigue life of LPBF Ti6Al4V(ELI) specimens built in the z-direction at ambient temperature. The difference from Malefane et al. [15] study, and the present study is most likely due to differences in the values of maximum stresses. Other factors, such as differences in heat treatment procedures, may have contributed to this. The results show that temperatures below 325 °C have an insignificant influence on the fatigue behaviour of Ti6Al4V alloy. The alloy's components, such as compressor blades and discs, exhaust valves, and fasteners, which are applied at temperatures below 325 °C, remain appropriate to be used at such elevated temperatures. At temperatures below 175 °C, the alloy's components, such as landing gears and wings in aircraft, biomedical implants, and the body and connecting rods of automobiles [12], remain suitable for their current application.

Specimens 1, 2, 3, and 4 were taken for porosity analysis on the micro-CT scanner. The dimensions of a larger pore that could cause failure were taken. The formula for change in stress intensity was used to determine their respective values of stress intensity. It is not surprising that specimen 1, which was tested at room temperature and at the highest maximum stress with a greater area of defect, had the greatest value of change in stress intensity factor. This high value of ΔK, led to the sole failure of all the tested specimens. For specimens that were tested at higher temperatures, it can be noted that specimen 3 has a higher value of ΔK, than specimen 4, though the area of defect was less. This is because specimen 3 was tested at a higher maximum test stress than specimen 4. On the other hand, specimen 2, with a smaller defect area, was tested at a higher maximum test stress than specimens 3 and 4, and has a small value of ΔK. For this case, elevated temperatures could have influenced this.

3.2. Fractography

Following tension-tension fatigue testing, the specimens were taken for scanning electron microscope fracture analysis. The SEIs fracture surface of specimen 1, which was tested at 20 °C, stressed to a maximum stress of 666.6 MPa, and failured after 373,193 cycles, is shown in Figure 2.

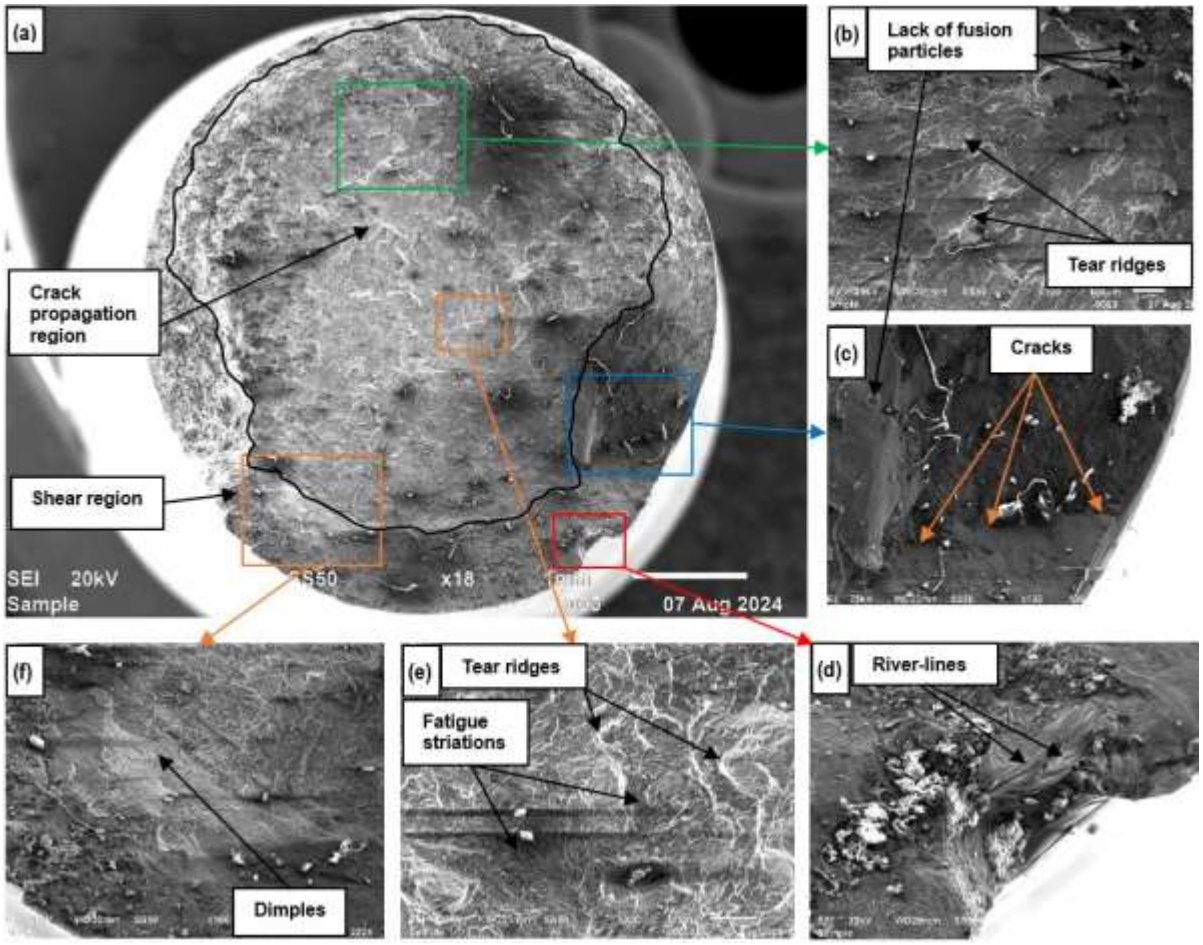


Figure 2: SEIs of the fracture surface of a specimen that was tested at 20 °C

The overall micrograph of one-half of a cup-and-cone fracture is shown in Figure 2(a). Three areas of porosity are evident in the micrograph. The first area exhibits a lack-of-fusion defect, as indicated by a green outline on the micrograph, covering an area of 0.027 mm². Powder that is not completely melted causes lack-of-fusion pores to form [16]. The second area, indicated by a blue boundary, has cracks near the surface and lack-of-fusion pores. Compared to gas pores, these pores have a more detrimental effect on fatigue life. The specimen's surface has an open pore or surface defect in the third location, which is highlighted in red, has an area of 0.036 mm^2. This pore may significantly impair fatigue performance. Unmelted powder particles with spherical shapes are shown in Figure 2(b), which is a greater magnification of a chosen region in Figure 2(a). Tear ridges are also shown in the figure. These tear ridges are visible throughout the crack propagation area shown in Figure 2(a). Figure 2(c) shows unmelted powder particles along with cracks. The figure shows a cleavage fracture feature with river-line patterns. Figure 2(d) shows a higher magnification of a region with an open-pore defect in Figure 2(a). The figure illustrates both fracture-related features and river-line patterns. A higher magnification of the fracture propagation area with tear ridges, fatigue cracks, and fatigue striations is shown in Figure 2(e). These fatigue striations show how a fatigue crack grows. Figure 2(a) shows the shear zone at a higher magnification, and Figure 2(f) shows the presence of quasi-cleavage fractured dimples. It can be concluded from the foregoing observations that failure in specimen 1 was significantly influenced by the high incidence of porosity, which explains why it failed alone whereas other specimens tested at room temperature did not.

3.3. Micro-CT Scanning

Specimens that endured 5,000,000 cycles without failure were taken for analysis on a micro-CT scanner. Figure 3 shows the micro-CT scanning of the fatigue specimens at the gauge section. The specimens are grey in colour, while the pores exhibit a variety of colours, ranging from large defects in pink to smaller defects in purple, as shown in Figs. 3.

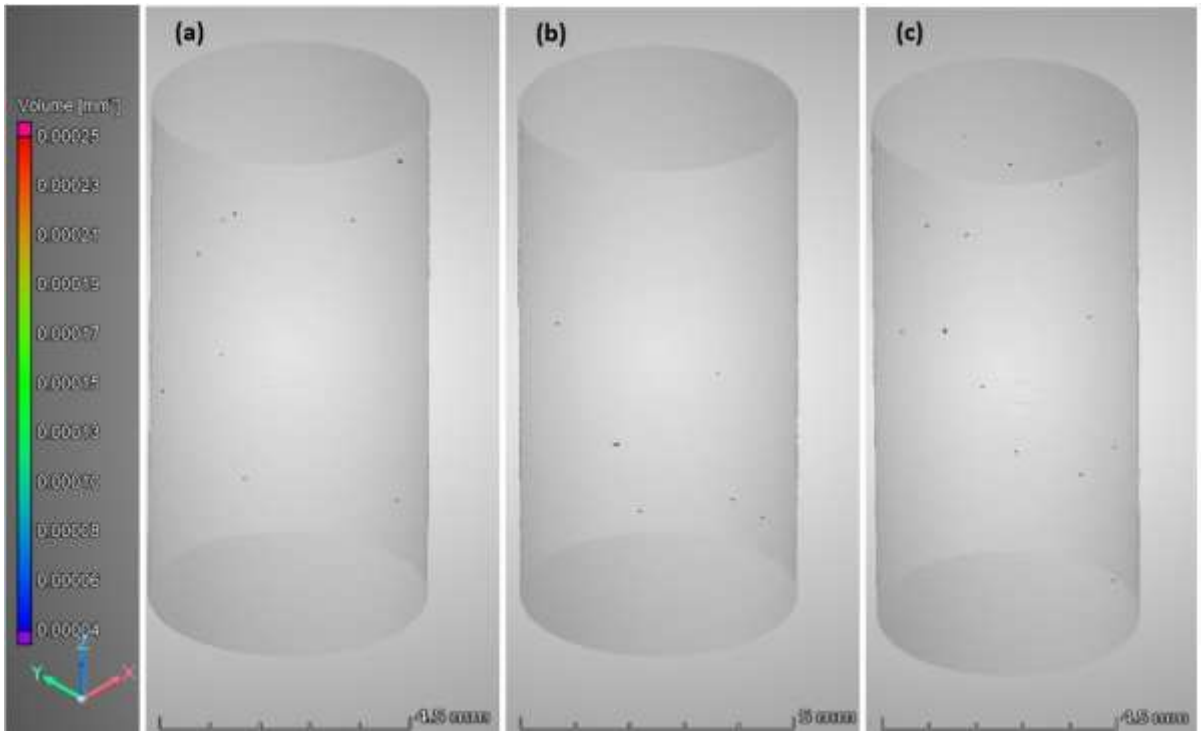


Figure 3: Micro-CT scanning image of the fatigue specimens that were tested at temperatures of (a) 20 °C, (b) 175 °C, and (c) 325 °C, at gauge sections

It is evident in Figure 3 that the level of porosity is low, with few pores scattered across the entire gauge section. Moletsane et al. [17], recorded a high density greater than 99.9% for LPBF Ti6Al4V(ELI) samples. Figure 3(a) shows approximately 9 pores, with the largest pore area measuring 0.019 mm² and the smallest measuring 0.029 mm². Figure 3(b) has six pores, with the largest and smallest pore areas of 0.032 mm² and 0.007 mm², respectively. In Figure 3(c), pores range in area from 0.005 mm² to 0.035 mm². These pores are quite small, implying that they were insufficient to cause stress concentration and ultimately failure within the specified (5,000,000) number of cycles. Furthermore, the sphericity of these pores is high (0.2 to 0.48). Li et al. [18], stated that stress concentration is more likely to occur in irregular pores as opposed to spherical pores. These irregular pores lower the specimen's mechanical performance. Defects cause stress concentration, which facilitates the initiation and growth of cracks, and reduces the samples' fatigue performance [14].

3.4. Microstructures

The microstructures of an LPBF Ti6Al4V (ELI) sample tested at room temperature, with a maximum stress of 666.6 MPa and 373,931 cycles of fatigue before fracture, are shown in Figure 4. Micrographs were taken from this specimen near the fatigue fracture surface and a distance of 25 mm away from the fracture surface.

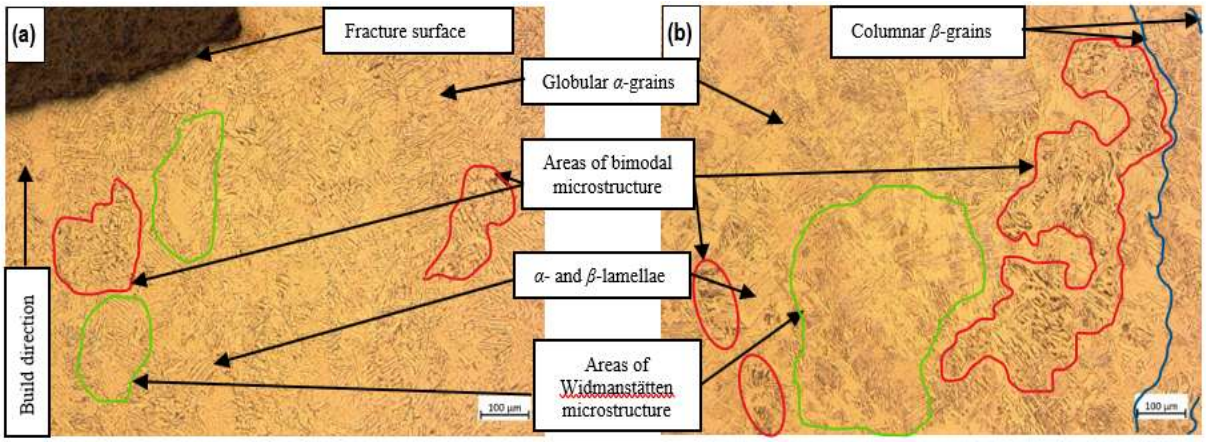


Figure 4: Optical micrograph of LPBF Ti6Al4V(ELI) samples (a) near the fatigue fracture area and (b) 25 mm away from the fracture area

Figure 4(a) shows the specimen's fracture surface. This micrograph's upper left corner displays the microstructure near to and on the specimen's edge. Lamellae microstructure, formed by α- and β-laths parallel to each other are evident in the figure. The micrograph shows the Widmanstätten microstructure, which is surrounded by green-coloured outlines. The micrograph shows areas of bimodal microstructure, which are indicated by red-coloured boundaries. The microscope also shows globular α-grains. The α- and β-laths in this micrograph had average widths of 7.4±0.4 µm and 1.2±0.2 µm, respectively. Figure 4(b) shows the microstructure of the fatigue sample on the grip section at a distance of 25 mm from the fracture surface. This micrograph shows the Widmanstätten microstructure as well as α- and β-lath lamellae. The bimodal microstructure is also evident and is shown encircled inside red colour boundaries on the micrograph. The blue line in the figure represents a columnar β-grain that contains colonies of α- and β-laths. This micrograph's α- and β-laths had average widths of 6.7±0.3 µm and 1.1±0.3 µm, respectively. The enlarged widths of the α- and β-laths in Figure 4(b) may have been caused by deformation processes that generated heat during fatigue fracture, which is thought to be the reason for the difference in the average widths of these two figures.

3.5. Vickers Microhardness

The average Vickers hardness values of the fatigue are shown in Table 3.

Table 3: Statistical values of Vickers hardness at different distances from the fracture surface

Distance from the fracture surface (µm)	Average hardness (HV)	Standard deviation	Coefficient of variance (%)	Total change in hardness from far distance hardness (%)
20	300.1	22.1	7.4	5.8
120	299.7	29.1	9.7	5.9
220	307.9	19.3	6.2	3.4
320	314.1	14.3	4.5	1.4
420	318.7	13.2	4.1	0.0
25000	318.6	11.9	3.7	0

An as-built Ti6Al4V alloy part has an average hardness of 362 HV [19]. Table 3 demonstrates that the alloy's hardness was considerably lowered to 318 HV by high-temperature annealing heat treatment. Table 3 clearly indicates that the average Vickers microhardness values, rounded to the nearest whole number, were constant at first, then increased continuously increasing distance from the fracture surface before remaining constant (at about 318 HV) after 420 µm. This trend suggests that the severity of deformation during fracture is dependent on the hardness of the tested Ti6Al4V (ELI) specimens. 9.7% was found to be the greatest CoV for the values shown in this table. The acquired data was moderately distributed from the mean and from one another, due to this moderate CoV.

Figure 5 shows the plotted average Vickers microhardness values given in Table 3.

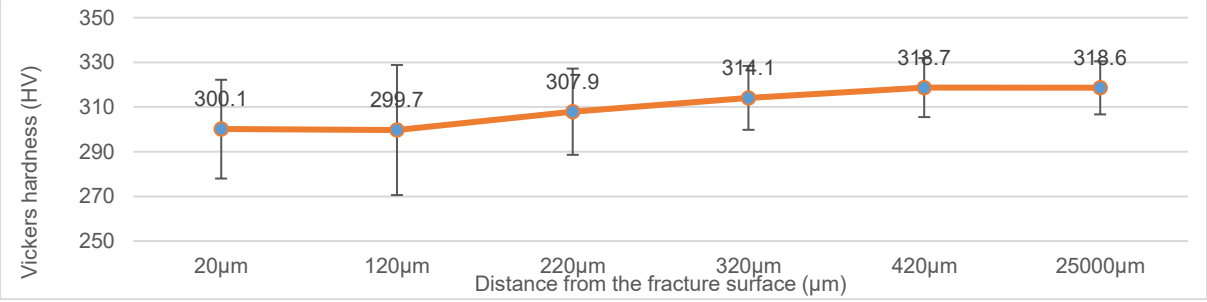


Figure 5: Vickers hardness average values for specimen 1 that was tested in tension-tension fatigue at 20 °C

Figure 5 shows a direct relationship between the mean values of hardness and distance away from the fracture surface, with the exception of points between distances of 20 μm and 120 μm, as well as 420 μm and 25,000 μm, away. As we proceed away from the fracture surface, the hardness values remain constant for a time, increase up to a distance of 420 μm, and then remain constant beyond that. The curve confirms the findings made on the results shown in Table 3. The results indicate that fatigue-induced fracture did influence the alloy's hardness, but the significance of this effect is questionable because the determined average values were all within each other's error bars.

Conclusions

This paper aimed to investigate the effect of elevated temperatures on the fatigue behaviour of high-temperature annealed Ti6Al4V(ELI). The results showed that:

- Maximum stresses below 583.2 MPa did not result in failure.
- Test temperatures below 325 °C did not affect the fatigue behaviour.
- Fracture occurred gradually and steadily for the sole fractured specimen.
- The stress intensity threshold adopted from literature was lower than the calculated values of the stress intensity factor.
- The average widths of α- and β-laths increased due to the severity of fracture, as the widths were marginally wider near the fatigue fracture surface.
- The average values of Vickers microhardness decreased slightly because of the degree of fracture, as the average values of hardness were lowest closer to the fracture.
- The micro-CT scans of LPBF samples revealed a low degree of porosity, and the material's density was greater than 99.9%.

Funding Details

This work was financially supported by the South African Department of Science and Innovation (DSI) through the Collaborative Program in Additive Manufacturing (CPAM) (Contract no CSIR-NLC-CPAM-21-MOA-CUT-03) and the Central University of Technology Free State's Research Grants and Scholarship Committee. The University of South Africa (UNISA), the University of the Free State (UFS), the University of Stellenbosch, the Product Development Technology Station (PDTS), and the Centre for Rapid Prototyping and Manufacturing (CRPM), are acknowledged for fatigue testing, micro-CT scanning, fracture analysis, machining, and production of the Ti6Al4V(ELI) specimens, respectively.

Disclosure Statement

The authors declare that they have no known competing financial interests or personal relationships that could have appeared to influence the work reported in this paper.

References

[1] E. A. Basuki, D. H. Prajitno, and F. Muhammad, "Alloys developed for high temperature applications," in AIP Conference Proceedings, American Institute of Physics Inc., Jan. 2017. doi: 10.1063/1.4974409.

[2] Y. ZHU, J. XIONG, Z. LV, and Y. ZHAO, "Testing and evaluation for fatigue crack propagation of Ti-6Al-4V/ELI and 7050-T7452 alloys at high temperatures," Chinese Journal of Aeronautics, vol. 31, no. 6, pp. 1388–1398, Jun. 2018, doi: 10.1016/j.cja.2017.06.013.

[3] K. Tokaji, "High cycle fatigue behaviour of Ti–6Al–4V alloy at elevated temperatures," Scr. Mater., vol. 54, no. 12, pp. 2143–2148, Jun. 2006, doi: 10.1016/J.SCRIPTAMAT.2006.02.043.

[4] N. K. Arakere, T. Goswami, J. Krohn, and N. Ramachandran, "High Temperature Fatigue Crack Growth Behavior of Ti-6A1-4V."

[5] Z. H. Jiao, R. D. Xu, H. C. Yu, and X. R. Wu, "Evaluation on Tensile and Fatigue Crack Growth Performances of Ti6Al4V Alloy Produced by Selective Laser Melting," in Procedia Structural Integrity, Elsevier B.V., 2017, pp. 124–132. doi: 10.1016/j.prostr.2017.11.069.

[6] ASTM International, "Standard specification for Additive Manufacturing Titanium-6 Alumium-4 Vanadium ELI (Extra Low Interstial) with Powder Bed Fusion," West Conshohocken, 2014.

[7] T. H. Becker, M. Beck, and C. Scheffer, "14 th International RAPDASA conference held at the Central University of Technology in South Africa in 2013," 2013.

[8] A. Dehghanghadikolaei and B. Fotovvati, "Additive Manufacturing Methods A Brief Overview," 2018. [Online]. Available: https://www.researchgate.net/publication/327701079

[9] A. E. Patterson, S. L. Messimer, and P. A. Farrington, "Overhanging Features and the SLM/DMLS Residual Stresses Problem: Review and Future Research Need," Technologies (Basel)., vol. 5, no. 4, p. 15, Apr. 2017, doi: 10.3390/technologies5020015.

[10] S. Liu and Y. C. Shin, "Additive manufacturing of Ti6Al4V alloy: A review," Mater. Des., vol. 164, p. 107552, Feb. 2019, doi: 10.1016/J.MATDES.2018.107552.

[11] A. Sterling, N. Shamsaei, B. Torries, and S. M. Thompson, "Fatigue Behaviour of Additively Manufactured Ti-6Al-4 v," in Procedia Engineering, Elsevier Ltd, 2015, pp. 576–589. doi: 10.1016/j.proeng.2015.12.632.

[12] J. R. Zhao, F. Y. Hung, T. S. Lui, and Y. L. Wu, "The relationship of fracture mechanism between high temperature tensile mechanical properties and particle erosion resistance of selective laser melting Ti-6al-4v alloy," Metals (Basel)., vol. 9, no. 5, May 2019, doi: 10.3390/met9050501.

[13] Yukitaka Murakami, "Metal Fatigue: Effects of Small Defects and Nonmetallic Inclusions," 2002.

[14] T. Moloi, T. C. Dzogbewu, M. Maringa, and A. Muiruri, "A Review of the Fatigue Behaviour of Laser Powder Bed Fusion Ti6Al4VA Review of the Fatigue Behaviour of Laser Powder Bed Fusion Ti6Al4V," Metallurgical and Materials Engineering, vol. 31, no. 1, pp. 288–310, Mar. 2025, Accessed: Oct. 29, 2025. [Online]. Available: https://metall-mater-eng.com/index.php/home/article/view/1245

[15] L. B. Malefane, W. B. du Preez, M. Maringa, and A. du Plessis, "Tensile and high cycle fatigue properties of annealed TI6AL4V (ELI) specimens produced by direct metal laser sintering," South African Journal of Industrial Engineering, vol. 29, no. 3 Special Edition, pp. 299–311, 2018, doi: 10.7166/29-3-2077.

[16] W. H. Kan et al., "A critical review on the effects of process-induced porosity on the mechanical properties of alloys fabricated by laser powder bed fusion," Jun. 01, 2022, Springer. doi: 10.1007/s10853-022-06990-7.

[17] M. G. Moletsane, P. Krakhmalev, N. Kazantseva, A. du Plessis, I. Yadroitsava, and I. Yadroitsev, "Tensile properties and microstructure of direct metal laser-sintered Ti6Al4V (ELI) alloy," South African Journal of Industrial Engineering, vol. 27, no. 3SpecialIssue, pp. 110–121, 2016, doi: 10.7166/27-3-1667.

[18] G. Li, P. Hu, G. Chen, M. Chen, and T. Yu, "Micro-pores formation mechanism and porosity on the fatigue performance of dual laser-powder bed fusion of Ti6Al4V," Int. J. Fatigue, vol. 199, p. 109077, Oct. 2025, doi: 10.1016/j.ijfatigue.2025.109077.

[19] T. D. Moloi, T. C. Dzogbewu, M. Maringa, and A. M. Muiruri, "The Effect of Temperature on the Microstructures of Additively Manufactured Ti6Al4V(Eli)," Iranian Journal of Materials Science and Engineering, vol. 21, no. 3, Sep. 2024, doi: 10.22068/ijmse.3589.